Block Copolymers Hot Paper

How to cite: *Angew. Chem. Int. Ed.* **2021**, *60*, 24107–24115
International Edition: doi.org/10.1002/anie.202107039
German Edition: doi.org/10.1002/ange.202107039

# Distorted Sandwich α-Diimine $Pd^{II}$ Catalyst: Linear Polyethylene and Synthesis of Ethylene/Acrylate Elastomers

*Yu-Sheng Liu and Eva Harth**

***Abstract:*** *The introduction of m-xylyl substituents to α-diimine $Pd^{II}$ catalyst promotes living ethylene polymerization at room temperature and low pressure to yield high molecular weight polyethylene (PE) with low branching (<17/1000 C). m-Xylyl groups provide a highly effective blockage to the axial sites of the catalytic center and form a distorted sandwich geometry. The shielding prevents chain-transfer and easy accessibility of polar monomers, leading to a living polymerization. Conducting a light irradiation as part of the one-step metal-organic insertion light initiated radical (MILRad) process leads to diblock copolymers of ethylene and acrylates. Incorporation of different acrylate block sequences can significantly modify the mechanical and chemical properties of block copolymers which can be modulated to be a hard plastic, elastomer, or semi-amorphous polymer.*

## Introduction

Since Brookhart and co-workers reported that α-diimine $Ni^{II}$ and $Pd^{II}$ complexes exhibit a unique chain-walking mechanism in olefin polymerization and copolymerize specific polar monomers which poison Ziegler–Natta/metallocene catalysts, the further exploration of these catalysts has been unwavering.[1] Modifications of α-diimine ligands have been the main source to tailor polymer microstructures and polar monomer incorporation.[1h,k,2] Specifically, the addition of steric bulk to the axial sides to control the chain-walking capabilities[3] in diimine Pd catalysts has inspired several complex designs. With higher axial shielding, chain-transfer can be retarded relative to the rate of coordination polymerization, living polymerization and high molecular weight polymers can be obtained under much improved thermal stability. Furthermore, the chain-walking ability can be increased by decreasing ethylene trapping, as trapping and insertion are competitive with chain-walking, leading to highly branched polyolefins.

For example, a sandwich Pd catalyst **A**, reported by Brookhart and Daugulis yielded a higher branched PE (110–120/1000 C) than compared from the typical diimine $Pd^{II}$ **B** (95–100/1000 C).[4] In addition, the "sandwich" Pd catalyst (Figure 1, **A**) exhibited narrow dispersity ($M_w/M_n < 1.1$), indicative of living polymerization. Jian and Mecking added a ridged axial protective framework to a diimine Pd complex with a dibenzobarrelene backbone (**D**) and prevented associative displacement chain-transfer to produce an unexpectedly ultrahigh branched PE (220/1000 C) containing mostly methyl branches.[5] In Guan's catalyst, the axial blockage can not only reduce the usual preference for ethylene but significantly increase the incorporation of polar monomers (**C**).[6] That the effect of shielding through bulky *ortho N*-aryl substituents at the axial positions of the square planar complexes towards chain-walking and insertion of ethylene is more multifaceted than anticipated could be observed in work from Chen (**E**).[3b,7] Here, the group installed phenyl and even more bulky naphthalyl groups to the *ortho N*-aryl position. Those catalysts resulted in high molecular weight PE as expected but surprisingly yielded PE with relatively low branching (20–29/1000 C).[7] These results demonstrated that the addition of steric bulk can be used as a tool to gain access to a broader range of branching density reaching from highly amorphous to semi-crystalline polymers. So far, it could not be determined which steric and electronic design features are key factors in axial shielding to reverse the usual trend towards higher branching in PE.

In this work, we aimed to further investigate how steric bulk positioned at *ortho N*-aryl substituents can lead to an axial shielding of the metal center to attain living, linear PE. We hypothesized that the installment of steric rotation barriers, instead of adding additional bulk, will result in a more effective and stable shielding of the metal without a complete blockage to enable ethylene trapping but keeping the ability to retard the chain-transfer. It is our aim to preserve living polymerization without lowering the activity of the catalyst and slowing down the rate of insertion, leading

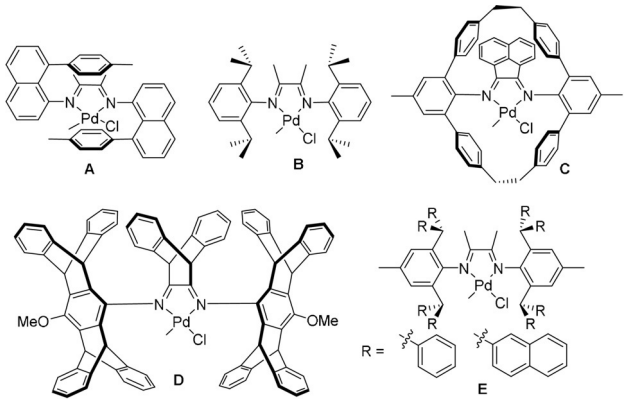


***Figure 1.*** Previous reported diimine Pd catalysts.

[*] Y.-S. Liu, Prof. Dr. E. Harth
Center of Excellence in Polymer Chemistry, Department of Chemistry, University of Houston
3585 Cullen Blvd, Houston, TX 77204 (USA)
E-mail: harth@uh.edu

Supporting information and the ORCID identification number(s) for the author(s) of this article can be found under: https://doi.org/10.1002/anie.202107039.

to limited chain-walking which results in semi-crystalline PE with high molecular weight.

The expansion of known diimine $Pd^{II}$ complexes to produce semi-crystalline PE is most valuable as the desired properties of PE stem mostly from its toughness and capability to organize into microdomains.[8] For example, the application of semi-crystalline PE as part of block copolymer architectures[9] is very attractive as the non-polar block asserts properties which polyacrylates alone are unable to achieve and vice versa. In our previous work, we have developed a one-step procedure of preparing polyolefin-polyacrylate copolymers called MILRad polymerization to join the complementary properties of these two monomer families.[10] These materials can work as interfacial reagents and have the ability to mix two polymers homogenously, like alloy. As block copolymers retain the features of each individual block, we are interested to combine semi-crystalline PE and polyacrylates to investigate the effect on the mechanical properties with a range of different acrylic monomers. To accomplish this goal, we sought to design a diimine $Pd^{II}$ complex which would show a high stability at ambient temperature, and provide a living behavior to be a viable candidate for MILRad polymerization.[10c] Moreover, a high molecular weight PE with a linear microstructure is most desirable to gain access to novel high molecular weight polyethylene/polyacrylate blocks with unexplored properties.[9d]

Herein, we report the design of two diimine $Pd^{II}$ complexes which examined the introduction of an effective rotation barrier through *meta*- and *para*-methyl groups at the benzhydryl substituents of diimine backbones in $Pd^{II}$ catalysts. The resulting sandwich catalysts with distorted square planar geometries at the metal center were investigated in polymerization with ethylene for their living behavior at low pressures and temperatures up to 80 °C, leading to high molecular weight PE with high linearity. Copolymerization with methyl acrylate (MA) gave further insight into the extend of the metal center shielding and differences resulting from the ligand design. One complex was selected to perform a MILRad polymerization to give a range of high molecular weight block copolymers with hard and soft, thermoplastic properties by tailoring the nature of the acrylic block.

## Results and Discussion

The preparation of the two complexes started with synthesis of the diimine ligands by forming two aniline derivatives through substitution reactions yielding **1a** and **2a**[11] followed by the synthesis of aniline derivatives **1b** and **2b**[12] through arylalkylation reactions. In an adapted reaction procedure, the two diimine ligands **1c** and **2c** were formed through a condensation reaction in high yields (Scheme 1). The following synthesis of the respective $Pd^{II}$ complexes was performed in chloroform with (COD)PdMeCl and yields 65 % for complex **1** with *m*-xylyl groups and 81 % for complex **2** with *p*-tolyl substituents in an updated procedure.

The X-ray structure of complex **1** (Figure 2, S60) and **2** (Figure S61) both exhibited slightly distorted square planar

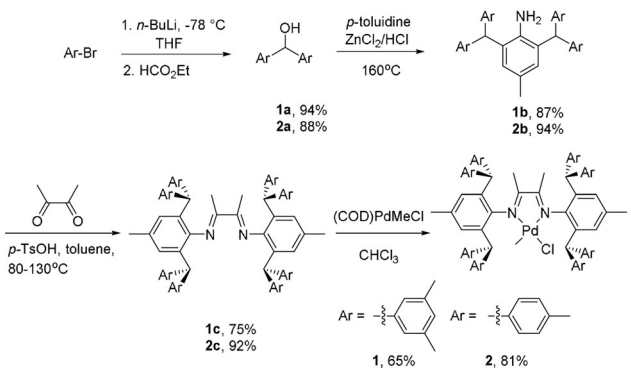


***Scheme 1.*** Synthesis of diimine $Pd^{II}$ complexes **1** and **2**.

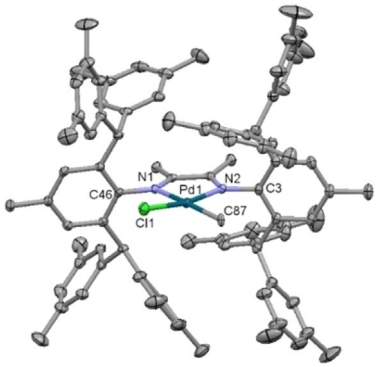


***Figure 2.*** Molecular structure of **1**. Hydrogen atoms are omitted for clarity. Ellipsoids are set at 50 % probability. Selected bond distances [Å] and angles [°]: Pd1–Cl1 2.3022(5), Pd1–C87 2.0762(19), Pd1–N1 2.1394(17), Pd1–N2 2.0467(17), N1–C46 1.433(3), N2–C3 1.446(3); N1-Pd1-N2 77.42(7), N1-Pd1-Cl1 98.52(5), N2-Pd1-C87 97.06(7).

geometries at the Pd center. The calculation for steric map[13] and buried volume $V_{Bur}$% of catalysts showed that $V_{Bur}$ of **1** is 60.4 % which is greater than the value of **2** (52.1 %) (Figure 3 b and e). Specifically, in complex **1**, the two *m*-xylyl rings cap the Pd like a distorted sandwich and the methyl substituents at the *meta* position of the phenyl rings are

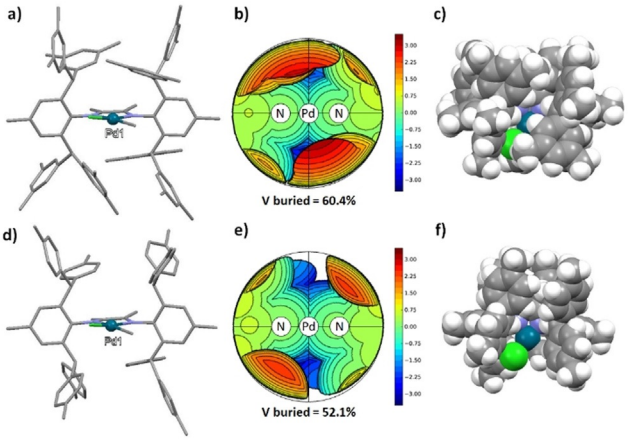


***Figure 3.*** a) Stick model of **1**; b) steric map and $V_{bur}$% of **1**; c) space-filling model of **1** (view from top to the bottom); d) stick model of **2**; e) steric map and $V_{bur}$% of **2**; f) space-filling model of **2** (view from top to the bottom).

  

***Table 1:*** Ethylene polymerization with catalyst **1** and **2**.[a]

| Entry | Cat. | $T$ [°C] | $t$ [min] | Yield [g] | Productivity [kg mol$_{Pd}^{-1}$ h$^{-1}$] | TOF [h$^{-1}$] | Branches/1000 C[b] | $M_n$[c] [kg mol$^{-1}$] | $M_w/M_n$[c] | $T_m$[d] [°C] | Crystallinity[d] [%] |
|---|---|---|---|---|---|---|---|---|---|---|---|
| 1 | **1** | 0 | 60 | 0.20 | 20 | 714 | 21 | 56.7 | 1.19 | 111.7 | 36.4 |
| 2 | **1** | 20 | 20 | 0.33 | 99 | 3536 | 19 | 89.3 | 1.14 | 111.2 | 34.3 |
| 3 | **1** | 40 | 15 | 2.92 | 1168 | 41 714 | 17 | 295.2 | 1.33 | 105.8 | 30.6 |
| 4 | **1** | 60 | 15 | 1.85 | 740 | 26 429 | 17 | 161.0 | 1.52 | 104.0 | 35.0 |
| 5 | **1** | 80 | 15 | 1.05 | 420 | 15 000 | 18 | 80.5 | 1.62 | 103.0 | 35.0 |
| 6 | **2** | 0 | 60 | 0.67 | 67 | 2393 | 21 | 98.7 | 1.07 | 112.4 | 36.3 |
| 7 | **2** | 20 | 20 | 1.72 | 516 | 18 429 | 19 | 233.4 | 1.09 | 104.5 | 27.3 |
| 8 | **2** | 40 | 15 | 1.83 | 732 | 26 142 | 20 | 215.2 | 1.27 | 99.2 | 27.5 |
| 9 | **2** | 60 | 15 | 1.77 | 708 | 25 286 | 23 | 68.0 | 1.58 | 90.6 | 34.7 |
| 10 | **2** | 80 | 15 | 0.98 | 392 | 14 000 | 25 | 36.2 | 1.76 | 89.2 | 36.4 |
| 11[e] | **1** | 25 | 60 | 2.22 | 222 | 7929 | 20 | 279.3 | 1.06 | 105.1 | 32.6 |
| 12 | **1** | 25 | 15 | 1.21 | 484 | 17 286 | 17 | 189.2 | 1.06 | 108.1 | 29.2 |
| 13[e] | **2** | 25 | 60 | 1.33 | 133 | 4750 | 21 | 160.1 | 1.10 | 103.2 | 28.1 |
| 14 | **2** | 25 | 15 | 1.37 | 548 | 19 571 | 18 | 212.5 | 1.11 | 104.3 | 34.8 |

[a] Conditions: 10 μmol of Pd catalyst, 1.2 equiv of NaBArF, 135 psi ethylene, 50 mL of chlorobenzene. [b] Determined by $^1$H NMR in $D_2$-tetrachloroethane at 125 °C. [c] Determined by SEC in 1,2,4-trichlorobenzene at 150 °C using triple detection. [d] Determined by differential scanning calorimetry. [e] 15 psi.

providing a rotation barrier which prove to be more shielding than at the *para* position (Figure 3a and d). The difference of axial shielding between **1** and **2** can be differentiated from the space-filling model. The axial sites of **1** were blocked by the ligand, but **2** displayed a more open structure (Figure 3c and f). Apparently, *m*-xylyl backbone provided efficient shielding and the Pd was buried by *m*-xylyl moieties.

To evaluate the effects of the geometries in the prepared complexes, we started with polymerization of ethylene using a Büchi glass Parr reactor and an in situ activation with 1.2 equivalents of sodium tetrakis(3,5-bis(trifluoromethyl)-phenyl)borate (NaBArF). Catalyst **1** and **2** were both highly active and robust in ethylene polymerizations in temperature ranges from 0 °C to 80 °C (Table 1). With increasing temperatures, the productivity and turnover frequency (TOF) of catalyst **1** and **2** also increased and reached their maximum at 40 °C. Catalyst **1** showed the lowest activity at 0 °C (TOF = 714 h$^{-1}$) and highest activity at 40 °C (TOF = 41 714 h$^{-1}$). In the overall temperature range between 0 °C to 80 °C, the activity of **1** significantly varied (Table 1, entry 1–5). The activity of catalyst **2** is almost constant between 20 °C and 60 °C (Table 1, entry 7–9), but the molecular weights of PE are decreasing when higher temperatures above 40 °C were applied. In comparison, PE molecular weights of catalyst **1** also reached the maximum together with TOF at 40 °C. The branching density of PE produced by catalyst **1** and **2** is around 20 branches per 1000 C which is relatively low compared to previously reported diimine Pd catalysts (Figure S13, S15). Even though xylyl groups in catalyst **1** providing a higher axial blockage compared to **2**, the difference in branching is only minor. The branching of PE generated from catalyst **1** is independent of the applied temperature, but slightly increases with raising temperatures when using **2**. Due to the high activity and low branching nature of catalyst **1** and **2**, PE from both catalysts appeared as white solid with a 35 % crystallinity and a melting temperature of around 110 °C.

To access the effect of applied pressure for ethylene polymerization a range of 135 psi and 15 psi (1 atmosphere) of was employed. When using 135 psi, both **1** and **2** exhibited high activity and yielded high molecular weight PE with narrow dispersities ($M_w/M_n < 1.1$). Surprisingly, catalyst **1** not only kept a high productivity at 15 psi of ethylene, but still yielded PE with high $M_n$ and very narrow dispersity ($M_w/M_n =$ 1.06) even when the polymerization was conducted for an hour at room temperature (Table 1, entry 11). The high temperature size-exclusion chromatography (HT-SEC) analysis also confirmed that no low $M_n$ of PE was generated by **1** during polymerization (Figure S31). Although, catalyst **2** yielded narrow dispersity PE, a small amount of low molecular weight PE was generated resulting from chain-transfer and confirmed by HT-SEC analysis (Figure S32). The $M_w/M_n$ values observed for experiments of **1** at 135 psi and 15 psi were both 1.06, which is fully consistent with a living polymerization behavior. The $^{13}$C NMR revealed that the branching distribution of PE from catalyst **1** are exclusively consisting of methyl groups and no long-chain branching was detected (Figure S14).

We demonstrated in this study that catalyst **1** and **2** with the phenyl based steric bulk promote a highly active diimine Pd complex producing linear PE through a hindered chain-walking ability of the complex and a higher insertion rate. However, living polymerization could be only facilitated by introducing a more effective blocking at the axial sites of the metal center, like observed in catalyst **1**. The less bulky structure but more rigid structure of the framework in complex **1** in contrast to other high steric bulk catalyst[7] might be responsible for the higher linearity and exclusive methyl branching formation in PE and extended livingness of this complex.

In the study of copolymerization with ethylene and MA (Table 2), different pressures of ethylene and concentrations of MA were employed. The initial experiments were conducted at 15 psi of ethylene and 1.0 M of MA solution at 25 °C for 2.0 h. (Table 2, entry 1 and 5). $^1$H NMR analysis of the copolymers showed the indicative signals for a MA incorporation with a singlet at 3.72 ppm which was identified as the

  

***Table 2:*** Ethylene/methyl acrylate copolymerization.[a]

| Entry | Cat. | $C_2H_4$ [psi] | [MA] [mol $L^{-1}$] | Yield [mg] | TOF [$h^{-1}$] | Branches/1000 C[b] | $M_n$[c] [kg $mol^{-1}$] | $M_w/M_n$[c] | Incorp[b] [mol %] | $T_m$[d] [°C] | $T_g$[d] [°C] |
|---|---|---|---|---|---|---|---|---|---|---|---|
| 1 | **1** | 15 | 1 | 53 | 95 | 19 | 27.8 | 1.75 | 0.56 | 112.0 | −22.8 |
| 2 | **1** | 50 | 1 | 126 | 225 | 20 | 42.3 | 1.78 | 0.11 | 112.0 | −8.4 |
| 3 | **1** | 50 | 2 | 44 | 79 | 18 | 25.8 | 1.68 | 0.26 | 112.9 | 12.4 |
| 4 | **1** | 135 | 5 | 46 | 82 | 20 | 16.6 | 2.09 | 0.17 | 112.1 | −7.7 |
| 5 | **2** | 15 | 1 | 71 | 127 | 24 | 6.5 | 1.40 | 1.65 | 107.0 | −15.6 |
| 6 | **2** | 50 | 1 | 218 | 389 | 17 | 15.8 | 2.22 | 0.24 | 111.3 | -1.5 |
| 7 | **2** | 50 | 2 | 128 | 229 | 22 | 6.2 | 1.96 | 0.21 | 107.2 | 9.1 |
| 8 | **2** | 135 | 5 | 47 | 84 | 34 | 2.2 | 1.89 | 0.25 | 102.7 | – |

[a] Conditions: 10 μmol of Pd catalyst, 1.2 equiv of NaBArF, 10 mL of chlorobenzene, 2 h, 25 °C. [b] Determined by $^1$H NMR in $D_2$-tetrachloroethane at 125 °C. [c] Determined by SEC in 1,2,4-trichlorobenzene at 150 °C using triple detection. [d] Determined by differential scanning calorimetry.

MA methyl ester group and multiplets present at 1.50–1.60 and 2.20–2.30 ppm as the peaks for MA methylene groups. The differential scanning calorimetry (DSC) analysis and glass transition temperature ($T_g$) measurements also indicated the formation of poly(ethylene-*co*-methyl acrylate), as a $T_g$ was not detected in ethylene homopolymers. The TOF of **1** and **2** were decreased to around 100 $h^{-1}$ which is one order of magnitude lower than without MA present (Table 1, entry 11,13). In addition, the MA incorporation of catalyst **2** reached 1.7 mol %, but a low molecular weight ethylene/MA copolymer (6.5 kg $mol^{-1}$) was generated. Copolymers from **1** showed only 0.5 mol % of MA incorporation, but the molecular weight was four times higher than with catalyst **2**. With ethylene pressure increased to 50 psi, the activity and molecular weight also increased, but the MA incorporation showed an opposite trend. The xylyl groups of catalyst **1** provided steric shielding for hindering the MA coordination and insertion. Overall, the axial blockage of xylyl groups retarded polar functional group binding to metal and chain-transfer, which is key to yield higher molecular weight copolymers. Based on the structural design of catalyst **2**, access of MA to the metal center is easier to achieve, which greatly decreases its activity and lower molecular weight copolymers are obtained.

The block copolymerization of ethylene and acrylate monomers was conducted by coordination polymerization of ethylene with catalyst **1**, and sequentially adding a selected acrylate monomer, followed by an irradiation with 450 nm blue light to generate the macroradical to initiate the free radical polymerization and forming the second polyacrylate bock segment (Scheme 2). From our previous work and discovery of MILRad,[10a,c] we have learned that a living polymerization of the olefin monomer is critical to enable a quantitative generation of polyolefin macroradicals as these originate from the homolytic cleavage of the Pd–C bond through light irradiation. Therefore, we selected complex **1** for the block copolymer synthesis as this catalyst showed living behavior without chain-transfer at room temperature and the ability to produce high molecular weight PE.

We first tested the block copolymerization of ethylene and MA. In a one-pot reaction, we used catalyst **1**, NaBArF, and applied a pressure of 135 psi of ethylene to synthesize the PE block. To minimize the chain-transfer product generated during polymerization, a controlled PE block was prepared with $M_w/M_n < 1.1$ and $M_n = 80$–$90$ kg $mol^{-1}$ in the living window of the complex in 10 min reaction time (Table 3, entry 1). MA was immediately introduced to the glass parr reactor to synthesize the PMA block sequence under light irradiation at 450 nm. After photoreaction, the composition of the block copolymer showed an overall 2 mol % MA content with a total molecular weight of $M_n = 107$ kg $mol^{-1}$ (Table 3, entry 1). In addition, the morphology of block copolymer was not amorphous but solid, similar to PE obtained from **1**, but appeared to be less brittle. Increasing the added amount of MA to 5.0 g (Table 3, entry 2), the entire block could be extended to 231 kg $mol^{-1}$ with a dispersity of $M_w/M_n = 1.35$. The incorporation of MA increased to 39 %, and the texture of the block copolymer appeared as a pliable but strong plastic. With increasing the feeding amount of MA to 10.0 g (Table 3, entry 3), the MA incorporation reached up to 63 %, and both molecular weight and dispersity also increased ($M_n = 552$ kg $mol^{-1}$, $M_w/M_n = 1.46$). Interestingly, we discovered that a significant shift to higher molecular weights between the PE block and PE-*b*-PMA diblocks in HT-SEC traces was not observed (Figure 4).

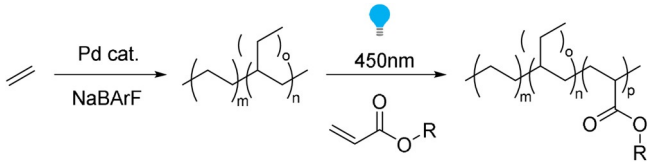


***Scheme 2.*** Synthesis of ethylene/acrylate block copolymers via MILRad.

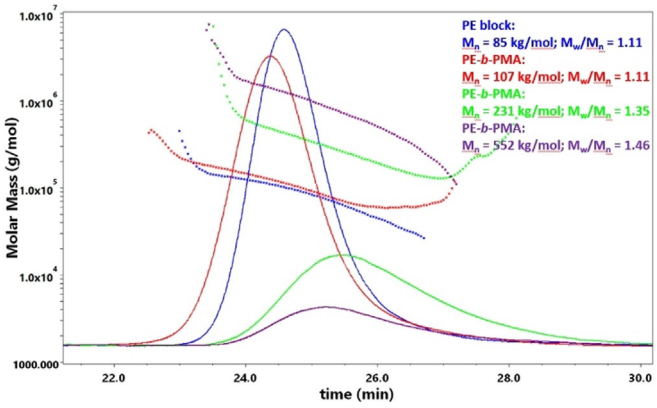


***Figure 4.*** HT-SEC traces of PE block and PE-b-PMA (entry 1–3, Table 3).

  

***Table 3:*** Ethylene/acrylate block copolymerization.[a]

| Entry | PE block | | Monomer[b] | Monomer | Yield | Branches/1000 C[c] | PE-*b*-P(acrylate) | | Incorp[c] | $T_m$[e] | $T_g$[e] |
|---|---|---|---|---|---|---|---|---|---|---|---|
| | $M_n$[d] [kg mol$^{-1}$] | $M_w/M_n$[d] | | [g] | [g] | | $M_n$[d] [kg mol$^{-1}$] | $M_w/M_n$[d] | [mol %] | [°C] | [°C] |
| 1 | 85.0 | 1.11 | MA | 1 | 0.38 | 18 | 107.1 | 1.11 | 2.0 | 110.3 | – |
| 2 | 80.6 | 1.13 | MA | 5 | 1.24 | 23 | 231.3 | 1.35 | 39.4 | 110.7 | 15.9 |
| 3 | 88.1 | 1.10 | MA | 10 | 2.38 | 19 | 552.3 | 1.46 | 62.6 | 109.7 | 14.8 |
| 4 | 80.4 | 1.10 | EA | 10 | 1.92 | 19 | 377.5 | 1.39 | 68.3 | 109.3 | −16.8 |
| 5 | 80.0 | 1.09 | *n*BA | 10 | 0.81 | – | 753.6 | 1.73 | 76.3 | 109.2 | −49.5 |
| 6 | 79.3 | 1.11 | *t*BA | 10 | 1.21 | – | 1519.2 | 2.03 | 62.7 | 107.7 | 49.9 |
| 7 | 79.2 | 1.09 | BzA | 10 | 2.84 | 19 | 922.9 | 1.11 | 77.7 | 106.8 | 9.4 |
| 8 | 88.5 | 1.08 | MMA | 10 | 0.46 | – | 208.6 | 1.51 | 30.4 | 109.8 | – |
| 9[f] | 16.0 | 1.16 | MA | 2 | 0.11 | – | 101.0 | 1.27 | 74.7 | 109.5 | 12.3 |

[a] Conditions: 10 µmol of **1**, 1.2 equiv of NaBArF, 50 mL of chlorobenzene, 135 psi ethylene, PE block 10 min, polyacrylate block 6 h, 25 °C. [b] Abbreviations: MA (methyl acrylate), EA (ethyl acrylate), *n*BA (*n*-butyl acrylate), *t*BA (*t*-butyl acrylate), BzA (benzyl acrylate), and MMA (methyl methacrylate). [c] Determined by $^1$H NMR in $D_2$-tetrachloroethane at 125 °C. [d] Determined by SEC in 1,2,4-trichlorobenzene at 150 °C using triple detection. [e] Determined by differential scanning calorimetry. [f] 20 µmol of **1**, PE block 2 min, polyacrylate block 3 h.

However, when analyzing the block copolymers by triple detection HT-SEC, the intensity of refractive index (RI) signals decreased with increased MA incorporation. This observation showed that the dn/dc of PE-*b*-PMA blocks decreased with increasing the molecular weight of the MA sequence and indicated the formation of high molecular weight copolymers. We hypothesize that the hydrodynamic volume of PE-*b*-PMA in trichlorobenzene is close to original PE block or even smaller.

The $^1$H NMR spectrum of PE-*b*-PMA exhibited not only multiplets of PE alkyl groups at 0.88–0.98 ppm and 1.10–1.48 ppm, but also a singlet of the MA methyl ester group at 3.73 ppm and four prominent multiplets of MA methylene in the PMA block at 1.55–1.65,1.74–1.80, 2.00–2.08, 2.36–2.48 ppm (Figure S20). DSC measurements of both PE-*b*-PMAs with 39 % and 63 % MA content showed the same crystalline melting temperature ($T_m$) and $T_g$ values ($T_m$ = 110 °C, $T_g$ = 15 °C) (Figure S47,48). The appearance and texture of the block containing 63 % PMA was similar to the 39 % PMA block, but with a higher MA content in the block sequence made the copolymer become more ductile and softer.

The MILRad polymerization technique could also be applied for the synthesis of other ethylene/acrylate block copolymers, including ethyl acrylate (EA), butyl acrylate (*n*BA), *tert*-butyl acrylate (*t*BA), benzyl acrylate (BzA), and methyl methacrylate (MMA). For these blocks (Table 3, entry 4–8, Figure S37-41), the same conditions to generate the PE block of $M_n \approx 80$ kg mol$^{-1}$ were applied and followed by addition of 10.0 g of the respective acrylates as described above for MA. It was found that the PE-*b*-PEA showed a high incorporation of EA (68 %), a high molecular weight ($M_n$ = 378 kg mol$^{-1}$) and moderate dispersity ($M_w/M_n$ = 1.39). Since the $T_g$ of PEA is much lower (−16.8 °C) than PMA (15.9 °C), PE-*b*-PEA displayed very different properties in contrast to the PE-*b*-PMA copolymer. The PE-*b*-PEA appears as a rubbery elastomer, whereas the MA copolymer was a hard plastic-like material but pliable. It is feasible that the $T_g$ of the polyacrylate block can significant modify the overall block copolymer properties. The following diblocks, PE-*b*-P*n*BA, PE-*b*-P*t*BA and PE-*b*-PBzA provided further information about the influence of $T_g$ towards material properties.

As observed in HT-SEC of PE-*b*-P*n*BA (Table 3, entry 5), the molecular weight of the block copolymer was significantly increased together with the dispersity which increased to 1.73. The $^1$H NMR spectrum of PE-*b*-P*n*BA exhibited all the prominent signals of the PE block and P*n*BA block. DSC analysis of the P*n*BA block showed a much lower $T_g$ of P*n*BA block (−49 °C) and PE-*b*-P*n*BA appeared as a semi-amorphous polymer. As for the PE-*b*-P*t*BA, the copolymer was a hard compact plastic and with no elastic behavior. The PE-*b*-PBzA was a pliable but a strong elastomer, and the elasticity was similar to PE-*b*-PEA but more tough and stiff. The PE-*b*-PMMA was not only a hard plastic, but exhibited tough, lightweight and glassy properties which originated from PMMA. As shown in entry 8, the block formation is much less efficient and lower yields are obtained than from the typical PE-*b*-PMA. Since the methyl group of MMA retards the radical to further react with monomers to propagate, the incorporation and yield of PE-*b*-PMMA is lower.

Notably, there was a significant shift in HT-SEC between PE block and PE-*b*-P*n*BA which was also observed for PE-*b*-P*t*BA, however not in any other blocks generated with PMA, PEA, PBzA, and PMMA blocks (Figure 5). The hydrodynamic volume of the butyl acrylate series is apparently different in the eluting solvent than of any other blocks in the series.

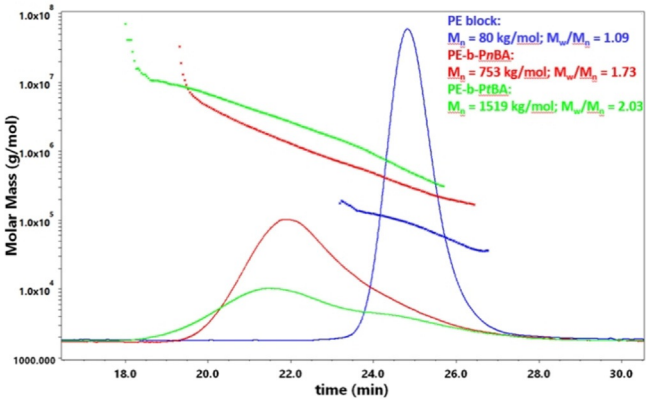


***Figure 5.*** HT-SEC traces of PE block, PE-*b*-P*n*BA and PE-*b*-P*t*BA (entry 5 and 6, Table 3).

  

To further confirm the formation of block copolymers, Diffusion ordered spectroscopy (DOSY) and Small-angle X-ray scattering (SAXS) were applied. The diffusion rate of DOSY depends on the hydrodynamic radius, molecular weight and temperature, therefore this technique is highly valuable to distinguish between block copolymers and mixtures of homopolymers. Since the prepared series of high molecular weight PE/polyacrylate blocks are only soluble in chlorinated solvents at high temperature, the distinct diffusion is challenging to be resolved. Therefore, we synthesized a PE-*b*-PMA (Table 3, entry 9) with a shorter PE block content ($M_n = 16\ kg\,mol^{-1}$) with high solubility at 40 °C. The DOSY spectrum showed the corresponding signals of the PE (1.28 ppm) and PMA block segment (3.68, 2.32, 19.6, 1.70 and 1.52 ppm), and aligned around a diffusion coefficient of $1.7 \times 10^{-13}\ m^2 s^{-1}$, which supported the formation of PE-*b*-PMA (Figure 6).

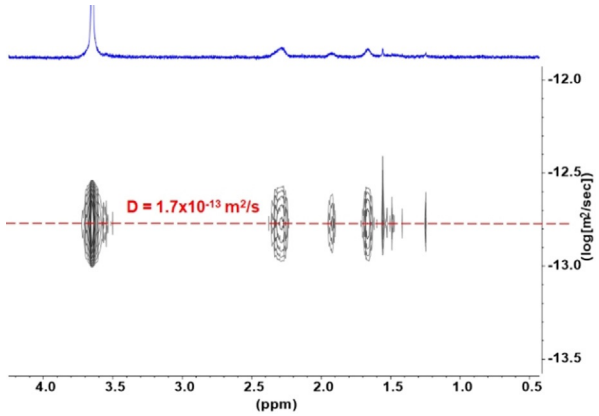


***Figure 6.*** DOSY $^1$H NMR spectrum of PE-*b*-PMA in $C_2D_2Cl_4$ at 40 °C (600 MHz) (entry 9, Table 3).

SAXS is also another technique to confirm the presence of block copolymers. Since PE and PMA are completely immiscible with each other, we expected microphase separation occurring in PE-*b*-PMA. The SAXS of PE-*b*-PMA showed a broad scattering at 120 °C which indicated a microstructure formation with no long-range order which supported the presence of blocks, in agreement with the MILRad mechanism. Notably, the scattering signal was detected at high temperature but not at 25 °C and the reason for this phenomenon is still unclear (Figure S54). We hypothesize that the crystallization of the semi-crystalline PE block might be prevented in the melt state and a microphase separation can be detected.

In our recent completed mechanistic study of MILRad,[10c] we proposed a mechanism for the block formation which detailed the investigation of the three critical parts of the block copolymer formation: the coordination-insertion polymerization, the photoinitiated "switch" and the radical polymerization. The insertion pathway leading to the polyolefin block is depicted in Scheme 3 and ethylene insertion and chain-walking results in the agostic intermediate **III** which can either proceed to undergo β-hydride elimination **IV** and chain-transfer **V** or undergo further coordination with monomers to form ethylene π complex **VI** to yield PE. In the so called "switch" phase an acrylic monomer coordinates **VII** and forms the macrochelates **VIII**, **IX** and **X**. As we have previously demonstrated, the predominantly stable six-membered chelate **X** needs the assistance of ancillary ligands to be ring opened to form the macroradical under light irradiation.[10c] However, in none of the block formations with MILRad using the complex **1**, the use of ancillary ligand was necessary. We hypothesize that when sterically demanding complexes such as complex **1** are used for block formation,

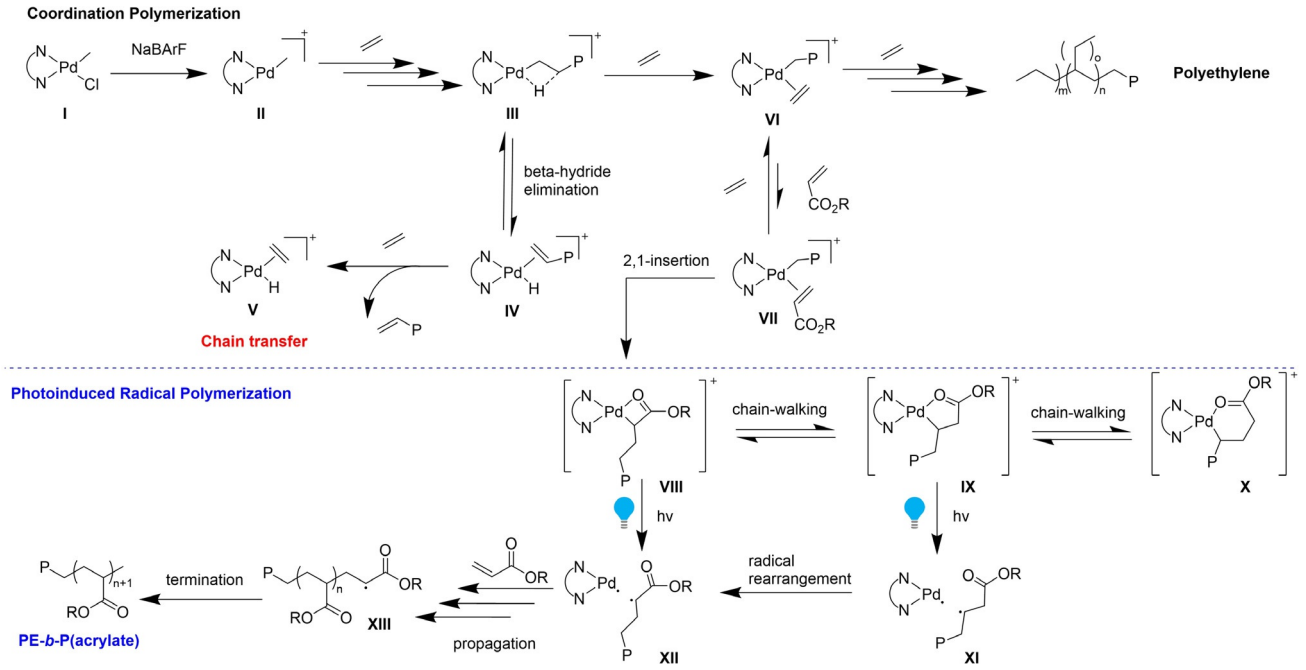


***Scheme 3.*** Proposed mechanism of block copolymer formation with complex **1**.

  

the four- **VIII** and five-membered macrochelates **IX** are more prevalent. These chelates can undergo Pd–C bond cleavage under light irradiation to form the α-carbonyl **XII** and β-carbonyl macroradical **XI** to proceed with the free radical polymerization pathway (Scheme 3). This updated version of the MILRad polymerizations is proposed for block copolymer syntheses that are performed with $Pd^{II}$ complexes with extensive axial shielding in contrast to the typical diimine $Pd^{II}$ catalysts.

Further chemical tuning and post-modification is made possible by the incorporation of active *N*-acryloyloxysuccinimide (NAS) ester groups.[14] In general, NAS functional groups enable the conjugation of primary amine-carrying entities, such as small molecules and (bio)-macromolecules. A block copolymer composed of PE (ca. 80 kg mol$^{-1}$) and a random copolymer of MA/NAS was prepared to give a block copolymer with 43 % active ester functionalization of the acrylate block and an 7 % overall active ester content (PE-*b*-P(MA-*co*-NAS), Figure 7 a, S28, 29). To demonstrate the ease of the post-functionalization process, a 1-pyrenemethylamine dye was conjugated to the activated groups and a green-blue emitting labeled block copolymer with a total molecular weight of $M_n = 170$ kg mol$^{-1}$ and $M_w/M_n = 1.08$ was formed (Figure 7 b, S30, S42).

We then carried out mechanical testing of PE and ethylene/acrylate block copolymers. PE obtained at 15 psi showed a strain at break of 306 % and a tensile strength of 16.7 MPa, while PE produced at 135 psi exhibited a more elastomeric behavior with an elongation break at 702 % and tensile strength of 31.6 MPa (Figure S55). The Young's modulus of both PEs showed a similar value and indicated that the material rigidity between both PEs is similar. A more detailed investigation of the mechanical properties by tensile stress testing confirmed the wide range of mechanical behavior of the PE/polyacrylate diblocks (Figure 8, S56,57). Interestingly, we found that polyacrylate blocks provide not only elastomeric properties, but also hardness and stiffness.

For example, the combination of P*t*BA or PMMA with PE blocks created rigid and hard and rigid copolymers. The PE-*b*-PMMA exhibited high tensile properties (tensile strength = 21.1 MPa, Young's modulus = 1300 MPa) and low deformation (strain = 3.6 %), as well as PE-*b*-P*t*BA (Figure S57). PE-*b*-PMMA exhibited a strain range up to 414 %, strength of

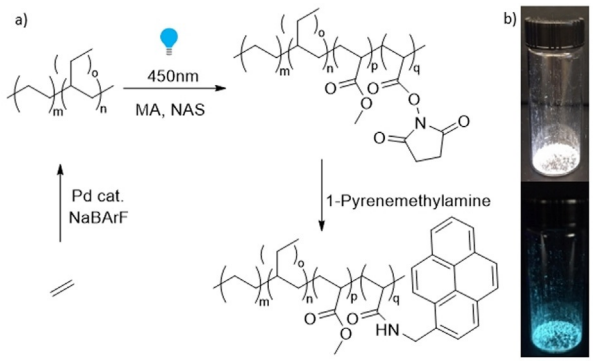


***Figure 7.*** a) Synthesis and post-modification of PE-*b*-P(MA-*co*-NAS). b) Emission of post-modified block copolymer upon 365 nm UV excitation.

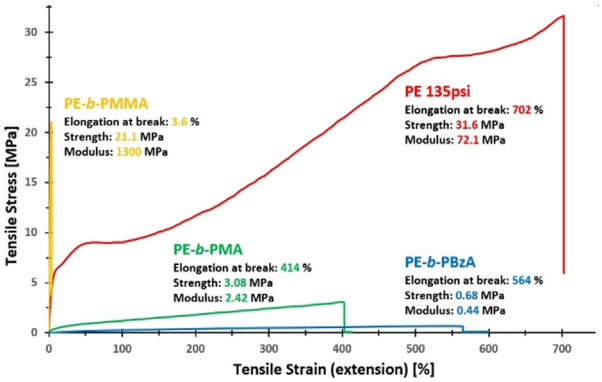


***Figure 8.*** Tensile testing of PE (entry 12, Table 1) and block copolymers (entry 3, 7 and 8, Table 3).

3.08 MPa, and a modulus of 2.42 MPa, but when the acrylate segment was changed to PEA, the strength decreased to 0.63 MPa (Figure 8, S56). The Young's modulus of PE-*b*-PEA dropped to 1.13 MPa and indicated deformation of PE-*b*-PEA is more facile than in PE-*b*-PMA. As for the P*n*BA and PBzA diblocks, both showed the same moduli, but great difference in strength and elongation. PE-*b*-P*n*BA could only encompass a strain to 53 %, but PE-*b*-PBzA gave elastomeric behavior with a strain at break of 564 %.

Cyclic stress–strain experiments were conducted to further test the elastic recovery of prepared crystalline elastomers. After the tensile strain reached 300 %, the sample of PE-*b*-PMA and PE-*b*-PBzA was unloaded fully, followed by a reloading (Figure 9). The tougher PE-*b*-PMA sample showed a 92.3 % recovery after unloading in contrast to the softer PE-*b*-PBzA which displayed a recovery of 93.1 %.

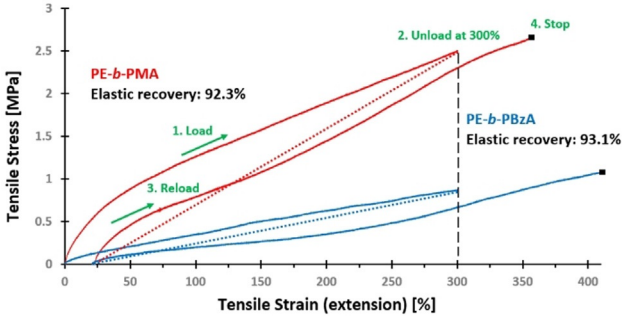


***Figure 9.*** Cyclic stress–strain test of PE-*b*-PMA and PE-*b*-PbzA.

These selected ethylene/acrylate diblock copolymers demonstrated that the mechanical properties can be tailored to a broad range of properties. To summarize, the blocks can be tuned to exhibit properties of a hard plastic, elastomer, or even semi-amorphous polymers. The crystalline nature of the low branching PE block provides hard and stiff properties and leads to elastomeric materials (PE-*b*-PMA and PE-*b*-PBzA) which are comparable to multiblock polyolefin materials.[15]

## Conclusion

Electronic and steric characteristics of axial shielding in α-diimine $Pd^{II}$ catalysts are considered to be the key governing factors to develop α-diimine catalysts which either produce amorphous or semi-crystalline polyolefins. Herein, we elucidate the effect of small methyl groups at *meta* or *para* positions of benzhydryl-derived substituents of the diimine backbone to function as rotation barriers to form catalyst geometries that balance shielding and monomer accessibility of the metal center. The results illustrated that *m*-xylyl substitutes form a distorted sandwich geometry which provide optimized conditions for a high catalytic activity and inhibition of chain-transfer to lead to the desired linear PE in living polymerizations of up to an hour. The high molecular weight PE is generated by catalyst **1** has not only a low branching density ($<17/1000$ C) but also consists solely of methyl branches. In comparison, *p*-tolyl groups exhibit a more open geometry of the catalyst **2** which leads to chain-transfer and non-living polymerizations. Copolymerization of ethylene with MA demonstrated further the profound effect of the two different geometric structures towards the accessibility of polar monomers. Catalyst **1** limits the availability of the catalytic center to MA and yields higher molecular weight ethylene/MA copolymers with a low polar monomer incorporation. In contrast, catalyst **2** incorporates MA more readily which greatly decreases its activity, and lower molecular weight copolymers are produced. The steric demands of catalyst **1** promotes an ethylene/acrylate block copolymer formation using the MILRad process without the addition of an ancillary ligand. A series of high molecular weight ($\approx 500$ K) block copolymers were generated. Furthermore, it was shown that a post-functionalization of block copolymers is feasible through the incorporation of NAS ester groups, demonstrated with an amine-carrying dye. The nature of the acrylic block could significantly modify the mechanical properties of PE and block copolymers ranging from elastomers to hard plastics were prepared. PE-*b*-PBzA and PE-*b*-PMA featured excellent elastomeric properties with high strain break values and elastic recovery which are further tested as additives for high performance plastics requiring strong interface interactions and impact strength.

## Acknowledgements

The authors thank the Robert A. Welch Foundation for generous support of this research (#H-E-0041) through the Center of Excellence in Polymer Chemistry and grant #E-2066-20210327. The authors are grateful to Dr. Xiqu Wang for collecting the diffraction data and solving X-ray structures, Dr. David T. Gillespie (Tosoh Bioscience) for helpful discussions about HT-SEC triple detection analysis, Dr. Scott K. Smith for helpful discussions about DOSY, Dr. Mateusz Janeta for helping with the topographic steric maps, Dr. Steve J. Swinnea (TMI, UT Austin) for SAXS measurement and Tatyana Makarenko for DSC measurements. The authors especially thank to Minjie Shen and Dr. Megan L. Robertson (UH Chemical Engineering) for their support in tensile testing measurements.

## Conflict of Interest

The authors declare no conflict of interest.

**Keywords:** block copolymers · copolymerization · elastomers · palladium catalysis · polyolefins

[1] a) L. K. Johnson, C. M. Killian, M. Brookhart, *J. Am. Chem. Soc.* **1995**, *117*, 6414 – 6415; b) C. M. Killian, D. J. Tempel, L. K. Johnson, M. Brookhart, *J. Am. Chem. Soc.* **1996**, *118*, 11664 – 11665; c) D. J. Tempel, L. K. Johnson, R. L. Huff, P. S. White, M. Brookhart, *J. Am. Chem. Soc.* **2000**, *122*, 6686 – 6700; d) L. H. Shultz, D. J. Tempel, M. Brookhart, *J. Am. Chem. Soc.* **2001**, *123*, 11539 – 11555; e) L. S. Boffa, B. M. Novak, *Chem. Rev.* **2000**, *100*, 1479 – 1493; f) F. Z. Wang, R. Tanaka, Q. S. Li, Y. Nakayama, T. Shiono, *Organometallics* **2018**, *37*, 1358 – 1367; g) K. B. Lian, Y. Zhu, W. M. Li, S. Y. Dai, C. L. Chen, *Macromolecules* **2017**, *50*, 6074 – 6080; h) L. K. Johnson, S. Mecking, M. Brookhart, *J. Am. Chem. Soc.* **1996**, *118*, 267 – 268; i) J. L. Rhinehart, L. A. Brown, B. K. Long, *J. Am. Chem. Soc.* **2013**, *135*, 16316 – 16319; j) F. Z. Wang, C. L. Chen, *Polym. Chem.* **2019**, *10*, 2354 – 2369; k) C. Tan, C. L. Chen, *Angew. Chem. Int. Ed.* **2019**, *58*, 7192 – 7200; *Angew. Chem.* **2019**, *131*, 7268 – 7276; l) Q. Muhammad, W. M. Pang, F. Z. Wang, C. Tan, *Polymers* **2020**, *12*, 2509.

[2] a) S. Mecking, L. K. Johnson, L. Wang, M. Brookhart, *J. Am. Chem. Soc.* **1998**, *120*, 888 – 899; b) Z. Chen, W. J. Liu, O. Daugulis, M. Brookhart, *J. Am. Chem. Soc.* **2016**, *138*, 16120 – 16129; c) Y. Kanai, S. Foro, H. Plenio, *Organometallics* **2019**, *38*, 544 – 551; d) A. Nakamura, S. Ito, K. Nozaki, *Chem. Rev.* **2009**, *109*, 5215 – 5244; e) W. C. Anderson, B. K. Long, *ACS Macro Lett.* **2016**, *5*, 1029 – 1033; f) B. K. Long, J. M. Eagan, M. Mulzer, G. W. Coates, *Angew. Chem. Int. Ed.* **2016**, *55*, 7106 – 7110; *Angew. Chem.* **2016**, *128*, 7222 – 7226; g) B. P. Carrow, K. Nozaki, *Macromolecules* **2014**, *47*, 2541 – 2555; h) S. Park, D. Takeuchi, K. Osakada, *J. Am. Chem. Soc.* **2006**, *128*, 3510 – 3511.

[3] a) L. H. Guo, S. Y. Dai, X. L. Sui, C. L. Chen, *ACS Catal.* **2016**, *6*, 428 – 441; b) S. Y. Dai, X. L. Sui, C. L. Chen, *Angew. Chem. Int. Ed.* **2015**, *54*, 9948 – 9953; *Angew. Chem.* **2015**, *127*, 10086 – 10091; c) Y. H. Zhao, S. K. Li, W. G. Fan, S. Y. Dai, *J. Organomet. Chem.* **2021**, *932*, 121649.

[4] K. E. Allen, J. Campos, O. Daugulis, M. Brookhart, *ACS Catal.* **2015**, *5*, 456 – 464.

[5] Y. X. Zhang, C. Q. Wang, S. Mecking, Z. B. Jian, *Angew. Chem. Int. Ed.* **2020**, *59*, 14296 – 14302; *Angew. Chem.* **2020**, *132*, 14402 – 14408.

[6] a) C. S. Popeney, C. M. Levins, Z. B. Guan, *Organometallics* **2011**, *30*, 2432 – 2452; b) D. H. Camacho, Z. B. Guan, *Chem. Commun.* **2010**, *46*, 7879 – 7893.

[7] S. Y. Dai, C. L. Chen, *Angew. Chem. Int. Ed.* **2016**, *55*, 13281 – 13285; *Angew. Chem.* **2016**, *128*, 13475 – 13479.

[8] a) P. J. Flory, D. Y. Yoon, *Nature* **1978**, *272*, 226 – 229; b) F. Liu, T. Sun, P. Tang, H. Zhang, F. Qiu, *Soft Matter* **2017**, *13*, 8250 – 8263; c) T. Y. Lu, K. Kim, X. B. Li, J. Zhou, G. Chen, J. Liu, *J. Appl. Phys.* **2018**, *123*, 015107.

[9] a) D. J. Walsh, E. Su, D. Guironnet, *Chem. Sci.* **2018**, *9*, 4703 – 4707; b) P. D. Goring, C. Morton, P. Scott, *Dalton Trans.* **2019**, *48*, 3521 – 3530; c) C. J. Kay, P. D. Goring, C. A. Burnett, B. Hornby, K. Lewtas, S. Morris, C. Morton, T. McNally, G. W. Theaker, C. Waterson, P. M. Wright, P. Scott, *J. Am. Chem. Soc.* **2018**, *140*, 13921 – 13934; d) A. Keyes, H. E. B. Alhan, E. Ordonez, U. Ha, D. B. Beezer, H. Dau, Y. S. Liu, E. Tsogtgerel, G. R. Jones, E.

  

Harth, *Angew. Chem. Int. Ed.* **2019**, *58*, 12370 – 12391; *Angew. Chem.* **2019**, *131*, 12498 – 12520.
[10] a) A. Keyes, H. E. B. Alhan, U. Ha, Y. S. Liu, S. K. Smith, T. S. Teets, D. B. Beezer, E. Harth, *Macromolecules* **2018**, *51*, 7224 – 7232; b) A. Keyes, H. Dau, H. E. B. Alhan, U. Ha, E. Ordonez, G. R. Jones, Y. S. Liu, E. Tsogtgerel, B. Loftin, Z. L. Wen, J. I. Wu, D. B. Beezer, E. Harth, *Polym. Chem.* **2019**, *10*, 3040 – 3047; c) H. Dau, A. Keyes, H. E. B. Alhan, E. Ordonez, E. Tsogtgerel, A. P. Gies, E. Auyeung, Z. Zhou, A. Maity, A. Das, D. C. Powers, D. B. Beezer, E. Harth, *J. Am. Chem. Soc.* **2020**, *142*, 21469 – 21483.
[11] Y. Gong, S. Li, Q. Gong, S. Zhang, B. Liu, S. Dai, *Organometallics* **2019**, *38*, 2919 – 2926.
[12] A. R. Martin, A. Chartoire, A. M. Z. Slawin, S. P. Nolan, *Beilstein J. Org. Chem.* **2012**, *8*, 1637 – 1643.
[13] L. Falivene, Z. Cao, A. Petta, L. Serra, A. Poater, R. Oliva, V. Scarano, L. Cavallo, *Nat. Chem.* **2019**, *11*, 872 – 879.
[14] A. Das, P. Theato, *Chem. Rev.* **2016**, *116*, 1434 – 1495.
[15] a) K. S. O'Connor, A. Watts, T. Vaidya, A. M. LaPointe, M. A. Hillmyer, G. W. Coates, *Macromolecules* **2016**, *49*, 6743 – 6751; b) D. J. Arriola, E. M. Carnahan, P. D. Hustad, R. L. Kuhlman, T. T. Wenzel, *Science* **2006**, *312*, 714 – 719.

Manuscript received: May 26, 2021
Revised manuscript received: July 29, 2021
Accepted manuscript online: August 17, 2021
Version of record online: October 5, 2021

  